

# Hints of Entanglement Suppression in Hyperon-Nucleon Scattering

Qiaofeng Liu<sup>1</sup> and Ian Low<sup>1,2</sup>

<sup>1</sup>*Department of Physics and Astronomy, Northwestern University, Evanston, IL 60208, USA*

<sup>2</sup>*High Energy Physics Division, Argonne National Laboratory, Argonne, IL 60439, USA*

Hyperon ( $Y = \Sigma, \Lambda$ )-nucleon ( $N = n, p$ ) interactions are crucial for understanding the existence of neutron stars heavier than two solar masses. Amid renewed experimental efforts, we study  $YN$  scatterings from the perspective of quantum information, focusing on whether spin entanglement is suppressed in the  $s$ -wave channel, which is observed in  $np$  scattering and leads to enhanced global symmetries. Using global fits of phase shifts from experimental data, we find hints of entanglement suppression among the eight flavor channels in the strangeness  $S = -1$  sector, similar to the  $np$  case. One exception is the  $\Sigma^+p$  channel, where conflicting global fits lead to inconclusive outcome. We then propose “quantum” observables in  $\Sigma^+p$  scattering to help resolve the differing global fits.

## I. INTRODUCTION

Understanding the dynamics of baryons is essential for obtaining a comprehensive picture of strong interactions, with broad implications in particle, nuclear, and astrophysics. While nucleon-nucleon interactions have been measured and constrained very precisely based on more than 4300 data points [1, 2], interactions involving baryons carrying strangeness quantum number – the hyperon – are much less understood, due to experimental difficulties associated with the short lifetime of hyperon and the challenges of preparing a stable hyperon beam. Very little experimental progress was made on  $YN$  scattering since the 1970s, until recently when the E40 collaboration at J-PARC and the CLAS collaboration at CEBAF announced new measurements [3–6]. Furthermore, there are also relevant measurements on  $YN$  interactions at the Large Hadron Collider from the ALICE collaboration recently [7, 8].

These new experimental efforts are driven, in part, by the “hyperon puzzle” in understanding the existence of neutron stars with a mass larger than two solar-mass [9, 10]. Neutron stars are compact objects supported against gravitational collapse by the Fermi degeneracy pressure of the neutron. However, in a dense environment the hyperon becomes stable because of the limited decay phase space and the Fermi pressure is reduced by the conversion of neutrons into hyperons due to the large chemical potential inside the neutron star, thereby softening the equation-of-state (EOS). Such a feature turns out to be incompatible with the observation of a neutron star heavier than two solar-mass [11, 12] as well as the stiff EOS measured by LIGO-Virgo [13, 14].

There has been continuous theoretical effort in describing  $NN$ ,  $YN$  and  $YY$  interactions over the years. Some popular approaches include meson-exchange potential models (the Nijmegen [15–17] and the Jülich [18, 19] potentials), the chiral effective field theory ( $\chi$ EFT) approach [20–22], and lattice QCD simulations (see the HALQCD [23, 24] and the NPLQCD [25, 26] collaborations). The underlying organizing principle is the  $SU(3)_f$  flavor symmetry among ( $u, d, s$ ) quarks, which is broken by quark masses. The spin-1/2 baryons, ( $n, p, \Sigma^\pm, \Sigma^0, \Lambda, \Xi^0, \Xi^-$ ), fill out an octet under  $SU(3)_f$ .

A major challenge is to incorporate  $SU(3)_f$  breaking effects in parameterizing  $YN$  and  $YY$  interactions amid constraints from the  $NN$  sector, and then extract useful information by fitting to the scarce data. Not surprisingly, ambiguities and inconsistencies among different approaches remain. Novel experimental techniques [27] and new theoretical insights are urgently needed.

Parallel to recent experimental advances, a new theoretical perspective was proposed in Ref. [28], which utilizes information-theoretic tools to analyze emergent symmetries in low-energy QCD. It was discovered that the S-matrix for  $np$  scattering below the pion threshold tends to suppress the spin-entanglement throughout the scattering, and such a suppression correlates with the emergence of Wigner’s  $SU(4)_{sm}$  spin-flavor symmetry [29] and the Schrödinger invariance [30] in the  $NN$  sector. Assuming  $SU(3)_f$  symmetry, Ref. [28] also studied the scattering between spin-1/2 baryons and found that entanglement suppression could give rise to an emergent  $SU(16)$  spin-flavor symmetry.

Building on the new insights, Ref. [31] analyzed the  $s$ -wave scattering of non-relativistic fermions from an information-theoretic setting and showed that the spin-flavor symmetry is associated with the S-matrix being interpreted as an Identity quantum logic gate and the Schrödinger symmetry is related to the SWAP gate. In Ref. [32] pathways to other emergent symmetries, such as  $SU(6)$ ,  $SO(8)$  and  $SU(8)$ , in baryon-baryon scatterings were pointed out. While the aforementioned physical systems are non-relativistic, recently the correlation between entanglement and symmetries was extended to a fully relativistic quantum system involving two-Higgs-doublet models and electroweak symmetry breaking, where a standard-model-like Higgs boson arises as a consequence of entanglement suppression [33].

Inspired by the advances in both experiment and theory, in this work we pursue a study on  $YN$  scattering from the viewpoint of quantum information. Our goal is two-fold: constrain the information-theoretic property of low-energy  $YN$  scattering using global fits of current data and propose quantum information-sensitive observables which may improve our understanding. Using the global fits is complementary to lattice QCD simulations, which assume  $SU(3)_f$  symmetry and sometimes adopt an unrealistic pion mass due to limited computing powers.

Pion production process	$p_{CM}$ (MeV/c)	$p_{lab}$ (MeV/c)
$\Lambda n \rightarrow \Lambda p \pi^-$	382.8	893.9
$\Sigma^+ p \rightarrow \Sigma^+ n \pi^+$	390.3	943.4

TABLE I. Representative pion production thresholds for  $YN$ .

$Q$	-1	0	1	2
Flavor	$\Sigma^- n$	$\Lambda n, \Sigma^0 n, \Sigma^- p$	$\Lambda p, \Sigma^0 p, \Sigma^+ n$	$\Sigma^+ p$
Total	2137	$\Lambda n : 2055$	$\Lambda p : 2054$	2128
Mass (MeV)		$\Sigma^0 n : 2132$ $\Sigma^- p : 2136$	$\Sigma^+ n : 2129$ $\Sigma^0 p : 2131$	

TABLE II. Eight flavor channel and the total mass in the strangeness  $S = -1$  sector, as labeled by the total charge  $Q$ .

## II. KINEMATICS

In the experimental setup, a beam of hyperon particles hit a stationary target, the nucleon. We label the incident particle mass as  $m_1$  and the stationary particle mass  $m_2$ . Masses of outgoing particles are represented by  $m'_1$  and  $m'_2$ . Experimental observables are usually measured as a function of the kinematic energy  $T_{lab}$  and the magnitude of the 3-momentum  $P_{lab}$  of the incident particle in the laboratory (Lab) frame. We will focus on the kinematic regime below the pion production threshold,

$$N_1 + N_2 \rightarrow N'_1 + N'_2 + \pi, \quad (1)$$

so that the interaction is described by the pionless effective field theory [34–37]. It is the easiest to calculate the pion threshold in the centre-of-mass (CM) frame which in terms of  $p_{CM}$ , the magnitude of the 3-momentum of the incident particle, is

$$p_{CM}^2 = \frac{[m'_1 m'_2 + (m'_1 + m'_2 + m_\pi/2)m_\pi]^2 - m_1^2 m_2^2}{(m_\pi + 2m'_1 + 2m'_2)m_\pi + (m_1 + m_2)^2}, \quad (2)$$

where  $m_\pi$  is the pion mass. In Table. I we list the representative pion production thresholds, in both the CM and the Lab frame, for  $YN$  scattering. The kinematic threshold in  $p_{CM}$  spans between (380, 390) MeV/c.

One interesting feature of  $YN$  scattering is the outgoing particles could have different flavors from the incoming particles, the flavor non-diagonal channels, in contrast with the  $NN$  scattering which is always flavor diagonal. In the limit of exact  $SU(3)_f$ , all spin-1/2 octet baryons are degenerate in mass and, since the strong interaction preserves the electric charge  $Q$  and the strangeness  $S$ , flavor channels within the same  $(Q, S)$  sector scatter only among themselves. For  $S = -1$  sector the flavor channels are classified according the electric charge  $Q$  in Table II. Notice that  $\Sigma^- n$  and  $\Sigma^+ p$  are unique in their respective  $(Q, S)$  sector, whose scatterings are always elastic and flavor diagonal.

In reality,  $SU(3)_f$  is broken and the baryons are not degenerate in mass. In Table II we also show the total mass of each  $YN$  channel, from which we see  $\Lambda p$  and  $\Lambda n$  are the lightest flavor channel in the  $Q = 0$  and  $Q = 1$

sectors respectively. This implies  $\Lambda p$  and  $\Lambda n$  would scatter elastically and flavor-diagonally until the kinematic thresholds for the next lightest flavor channels open up, which in  $(p_{CM}, P_{lab})$  are (279, 633) MeV/c for  $\Lambda p$  and (283, 633) MeV/c for  $\Lambda n$ , respectively.

## III. THE S-MATRIX

It is well-known that non-relativistic scatterings of spin-1/2 fermions in the low-energy are dominated by the  $s$ -wave channel, which contains the spin-singlet  $^1S_0$  and the spin-triplet  $^3S_1$  [31],

$$S = e^{2i\delta_0} P_s + e^{2i\delta_1} P_t, \quad (3)$$

where  $P_s$  and  $P_t$  are the spin-projectors into the  $^1S_0$  singlet and the  $^3S_1$  triplet channels, respectively,

$$P_s = \frac{1}{4} (1 - \boldsymbol{\sigma} \cdot \boldsymbol{\sigma}), \quad P_t = \frac{1}{4} (3 + \boldsymbol{\sigma} \cdot \boldsymbol{\sigma}), \quad (4)$$

and  $\boldsymbol{\sigma} \cdot \boldsymbol{\sigma} = \sum_a \sigma^a \otimes \sigma^a$ . Moreover,  $\delta_0$  and  $\delta_1$  are the scattering phase shifts which can be fitted from data.

The information-theoretic property of the S-matrix becomes transparent when we introduce the SWAP operator,  $\text{SWAP} = (1 + \boldsymbol{\sigma} \cdot \boldsymbol{\sigma})/2$ , which interchanges the spin of the two particles, and rewrite the S-matrix as [31],

$$S = \frac{1}{2} (e^{2i\delta_0} + e^{2i\delta_1}) 1 + \frac{1}{2} (e^{2i\delta_0} - e^{2i\delta_1}) \text{SWAP}. \quad (5)$$

It then becomes clear that the S-matrix in the spin subspace is an Identity operator in the spin-space if  $\delta_0 = \delta_1$  while it is the SWAP operator if  $|\delta_0 - \delta_1| = \pm\pi/2$ . It turns out that 1 and SWAP are the only two operators which suppress entanglement [31], which can be seen from the observation that, starting from an arbitrary spin-wave function  $|\psi\rangle$  that is unentangled,  $|\psi\rangle = |\psi_1\rangle \otimes |\psi_2\rangle$ , the Identity and the SWAP operators both produce an outgoing state that is also unentangled. Note that  $\text{SWAP}|\psi_1\rangle \otimes |\psi_2\rangle = |\psi_2\rangle \otimes |\psi_1\rangle$ . It is much less obvious that these are the only two two-qubit logic gates which suppress entanglement [31]. For a unitary operator, it is possible to quantify the ability of an operator to generate entanglement by defining the entanglement power (EP) [38, 39], which for the S-matrix in Eq. (3) is [28],

$$E(S) = \frac{1}{6} \sin^2(2\delta_0 - 2\delta_1). \quad (6)$$

It vanishes when  $\delta_0 = \delta_1$  (the Identity) or  $|\delta_0 - \delta_1| = \pm\pi/2$  (the SWAP).

For a non-unitary operator, however, the EP is not well-defined. This is the case when we consider inelastic  $YN$  scattering in the  $Q = 0$  and  $Q = 1$  sectors, where the S-matrix is three-dimensional in the flavor subspace, as can be seen in Table II. Therefore, the flavor-diagonal entry of the S-matrix by itself is not a unitary operator

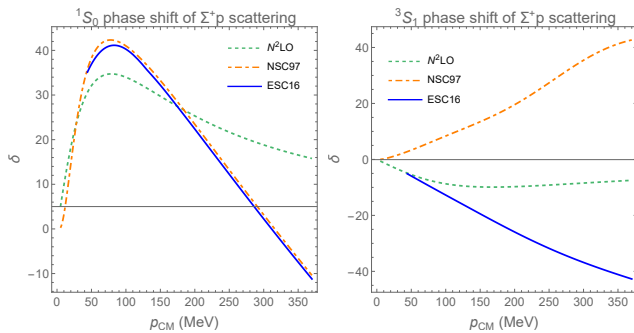


FIG. 1. Comparisons of phase shifts in the  $\Sigma^+p$  channel from potential models and  $N^2LO$   $\chi EFT$  ( $\Lambda = 500$  MeV), where only the scattering length  $a$  and the effective range  $r_0$  are included.

and it is customary to introduce the inelasticity parameter, which can also be extracted from data, for each flavor-diagonal channel [40],

$$[S]_{jj} = \cos(2\alpha_0^j) e^{2i\delta_0^j} P_s + \cos(2\alpha_1^j) e^{2i\delta_1^j} P_t, \quad (7)$$

where  $[S]_{jj}$  is the diagonal entry of S-matrix describing the scattering  $j \rightarrow j$  in the flavor subspace. Below the inelastic threshold the inelasticity parameters vanish, which is the case for  $\Lambda p$  and  $\Lambda n$  channels. Although the EP is not well-defined for  $[S]_{jj}$  in Eq. (7), one can still rewrite  $[S]_{jj}$  as

$$[S]_{jj} = c_1 1 + c_S \text{SWAP}, \quad (8)$$

$$c_1 = \frac{1}{2} \left[ \cos(2\alpha_0^j) e^{2i\delta_0^j} + \cos(2\alpha_1^j) e^{2i\delta_1^j} \right], \quad (9)$$

$$c_S = \frac{1}{2} \left[ \cos(2\alpha_0^j) e^{2i\delta_0^j} - \cos(2\alpha_1^j) e^{2i\delta_1^j} \right]. \quad (10)$$

Then  $[S]_{jj}$  suppresses spin entanglement when the inelasticity parameters and the phase shifts conspire in such a way that  $[S]_{jj} \sim 1$  or  $[S]_{jj} \sim \text{SWAP}$ .

#### IV. GLOBAL FITS

There are two types of global fits in the literature. One type provides the global fit for the momentum dependence of the phase shifts  $\delta_0(p)$  and  $\delta_1(p)$  in the  $^1S_0$  and  $^3S_1$  channels, from which we calculate the EP using Eq. (6). In particular, we focus on two different fits developed for different purposes: the Nijmegen soft-core model (NSC97) [15, 16, 41] and the Nijmegen extended-soft-core model (ESC16) [42, 43].

The main difference between these two models lies in the  $\Sigma^+p$  channel, the  $(Q, S) = (2, -1)$  and isospin  $I = 3/2$  sector, where the NSC97 model predicts an attractive force in the  $^3S_1$  channel while the ESC16 model predicts a repulsive force. Historically two-body  $\Sigma^+p$  interactions are fitted from binding energies of hypernuclei, which seem to prefer a strong repulsive interaction [17, 44]. However, extracting the two-body interaction

from hypernuclear data requires knowledge of the three-body  $YNN$  force, which plays an important role in understanding the hyperon puzzle inside the neutron star [45] and is not precisely determined. In the end, it is highly desirable to be able to independently determine the two-body  $\Sigma^+p$  interactions directly from scattering data. In this regard, the latest phase shift analysis from measurements at J-PARC does not seem to be able to resolve the difference between ESC16 and NSC97 [5]. Consequently we utilize both models in the present work. We will see that these two models make distinctive predictions on the entanglement property of  $\Sigma^+p$  scattering.

The second type of fits makes use of  $\chi EFT$ , which is pioneered by Weinberg [46, 47] and has been very successful in describing  $NN$  interactions. Applications of  $\chi EFT$  to  $YN$  interactions have progressed steadily over the years [20–22] and the state-of-the-art calculation now stands at next-to-next-to-leading order ( $N^2LO$ ) [48], which we use.

There are two features of  $\chi EFT$  which are distinctly different from the global fits utilizing the potential models such as NSC97 and ESC16. First,  $\chi EFT$  is an expansion of the potential in small momenta and pion masses, augmented with an appropriate power counting rule. As such there is an inherent cutoff of  $\chi EFT$ , which is usually taken to be  $\Lambda \sim 500$  MeV. This implies that, as the  $p_{CM}$  gets close to  $\Lambda$ , higher order effects become important and  $\chi EFT$  starts breaking down. Second,  $\chi EFT$  employs the effective range expansion (ERE) [49]:

$$p_{CM} \cot \delta = -\frac{1}{a} + \frac{1}{2} \Lambda^2 \sum_{n=0}^{\infty} r_n \left( \frac{p_{CM}^2}{\Lambda^2} \right)^n. \quad (11)$$

In the above  $a$  is the scattering length,  $r_0$  is the effective range,  $r_1$  is the shape parameter, etc.  $\chi EFT$  only provides global fits to the first two ERE parameters:  $a$  and  $r_0$  in each flavor and spin channel, from which we extract the full momentum dependence of the scattering phase shifts  $\delta_i$  in Eq. (3). In Fig. 1 we show a comparison of the phase shifts in the  $\Sigma^+p$  channel from the potential models and from  $\chi EFT$  via Eq. (11). We see that phase shifts from the two approaches start diverging at  $p_{CM} \sim 70$  MeV. Moreover, the  $^3S_1$  phase shifts in ESC16 and  $N^2LO$   $\chi EFT$  have a negative sign (repulsive force) while in NSC97 it has a positive sign (attractive force). In the isospin-related channel of  $\Sigma^-n$ , lattice simulations seem to also indicated a negative  $^3S_1$  phase shift [50].

#### V. RESULTS

Here we present the information-theoretic properties of two-body  $YN$  interactions. There are eight flavor channels, as shown in Table II. Among them we will only show the results for  $\{\Sigma^+p, \Sigma^0p, \Sigma^-p, \Lambda p\}$ , since isospin invariance relates them to the remaining four channels,  $\{\Sigma^-n, \Sigma^0n, \Sigma^-n, \Lambda n\}$ , and the results look very similar. Notice that, in the ultra-low momentum region where non-perturbative structures such as poles and resonances

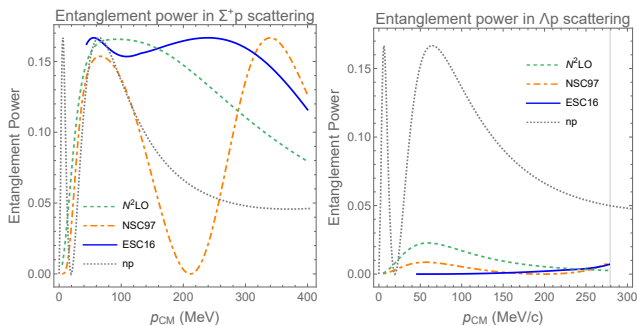


FIG. 2. EP in  $\Sigma^+p$  and  $\Lambda p$  channels, which are related to  $\Sigma^-n$  and  $\Lambda n$  channels, respectively, by isospin invariance. The EP for  $np$  scattering is included for comparison.

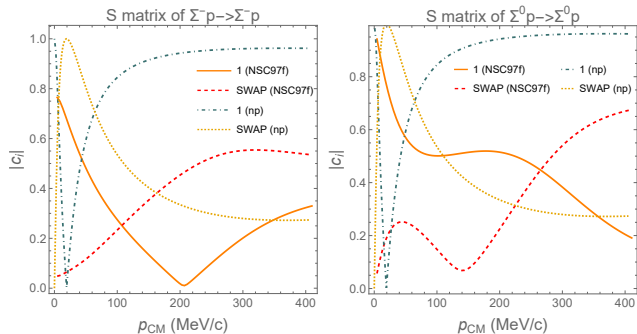


FIG. 3. S matrices in  $\Sigma^-p$  and  $\Sigma^0p$  channels, which are related to  $\Sigma^+n$  and  $\Sigma^0n$ , respectively, by isospin invariance. The S-matrix for  $np$  scattering is also shown.

dominate, the S-matrix could produce highly entangled states. Our interest lies in the regime above this infrared region,  $p_{CM} \gtrsim 100$  MeV, where nucleons and baryons can be considered as fundamental degrees of freedom.

There are two classes of results. The first involves elastic scatterings in the flavor-diagonal channels. They are  $\Lambda n$  and  $\Lambda p$  below the inelastic threshold at  $p_{CM} \sim 280$  MeV, as well as  $\Sigma^+p$  and  $\Sigma^-n$  below the pion production threshold at  $p_{CM} \sim 390$  MeV. (See Tables I and II.) In Fig. 2 we present the EP computed from Eq. (6) for  $\Sigma^+p$  and  $\Lambda p$  channels, and include the case of  $np$  scattering for comparison. We employ three global fits: NSC97, ESC16 and  $\chi$ EFT. In particular, NSC97 fits contain several versions [15, 16], among which we choose the NSC97f as a representative, although the conclusion does not depend on this choice. We see in Fig. 2 that the EP is highly suppressed in the region of  $p_{CM} \gtrsim 100$  MeV in the NSC97 fit for  $\Sigma^+p$  and in all three fits for  $\Lambda p$ . ESC16 and  $\chi$ EFT do not exhibit entanglement suppression in the  $\Sigma^+p$  channel due to the negative  $^3S_1$  phase shift, as shown in Fig. 1. In the  $\Sigma^-n$  and  $\Lambda n$  channels, only the NSC97 fit is available and the EP is suppressed in both channels, similar to their isospin partners.

The remaining channels,  $\{\Sigma^-p, \Sigma^0p, \Sigma^+n, \Sigma^0n\}$ , all scatter inelastically and we need to include the inelasticity parameters. In these cases we plot  $|c_1|$  and  $|c_S|$

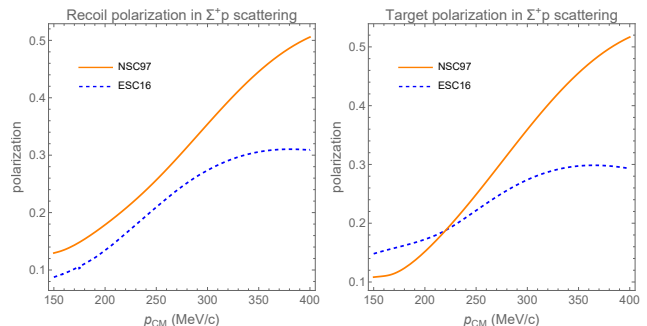


FIG. 4. Predicted polarizations of the recoiling  $\Sigma^+$  (recoil) and the recoiling  $p$  (target) in  $\Sigma^+p$  scattering, assuming an unpolarized proton target and a 25% polarized hyperon beam.

in Eqs. (9) and (10), which show the relative component of the S-matrix in 1 and SWAP. When the S-matrix is predominantly the Identity gate, or the SWAP gate, it suppresses entanglement. In Fig. 3 we present the results for  $\Sigma^-p$  and  $\Sigma^0p$  channels. The results for their isospin partners  $\Sigma^+n$  and  $\Sigma^0n$  look very similar. We again show the  $np$  case as a benchmark. Only the NSC97 fit is shown here, as the  $\chi$ EFT only provides fits for the scattering length, without the effective range [48]. We see that in  $\Sigma^-p$  channel the S-matrix is dominated by the SWAP gate at  $p_{CM} \sim 200$  MeV, while in  $\Sigma^0p$  channel it is dominated by the Identity gate at  $p_{CM} \sim 150$  MeV. Since the SWAP gate is associated with the Schrödinger symmetry [31], it would be interesting to further investigate the appearance of SWAP gate in these channels.

It is worth emphasizing that, even if one assumes  $SU(3)_f$  symmetry, these hints of entanglement suppression in  $YN$  interactions do not follow from the observed entanglement suppression in  $np$  scattering. In this limit, there are six  $SU(3)_f$  invariant phase shifts in the scattering of octet baryons and the phases entering  $np$  scattering are different from those appearing in  $YN$  scattering [32].

Given that, in the case of  $\Sigma^+p$ , different global fits give rise to inconclusive outcome, we further propose “quantum observables” which could not only distinguish the varying global fits but also help determine the density matrix of the outgoing states [51]. The observables are based on the formalism introduced in Ref. [52], which relates the density matrix of outgoing states to their polarizations. (For quantum observables in top quark decays, see Refs. [53, 54].) In Fig. 4 we plot the predicted polarizations, as a function of  $p_{CM}$ , of the recoiling hyperon (recoil polarization) and the recoiling proton (target polarization) in  $\Sigma^+p$  scattering from NSC97 and ESC16 fits, assuming an unpolarized proton target and a 25% polarized incoming hyperon beam. We see that, by measuring the recoil and target polarizations, it is possible to distinguish between the two global fits. At J-PARC the  $\Sigma^+$  particles come from the process  $\pi^+p \rightarrow \Sigma^+K^+$  and is partially polarized in the order of 25%, depending on the incoming momenta [55]. A more detailed study of such a scenario will be presented elsewhere [51].

## VI. CONCLUSION

Hyperon-nucleon interactions are important for resolving the “hyperon puzzle,” which pertains to the formation of neutron stars heavier than two solar-masses. Inspired by recent experimental efforts in direct measurements of  $YN$  scattering, as well as by theoretical advances in understanding nuclear dynamics from the perspective of quantum entanglement, we studied in this work the information-theoretic properties of two-body  $YN$  scatterings, focusing on the question of whether the spin entanglement is suppressed during the scattering process. Using global fits of scattering data, we find hints of entanglement suppression in the majority of  $YN$  scattering channels. In the case of  $\Sigma^+p$  scattering, conflicting global fits lead to inconclusive outcomes.

We further proposed polarizations of the recoiling hyperon and the recoiling proton as “quantum observables” which could determine the entanglement property of the

S-matrix. Such measurements could not only provide access to the density matrix of the outgoing states, but also help differentiate the conflicting global fits, which will have important implications for the hyperon puzzle as well. In addition, these observables open up new venues to investigate and measure the quantum nature of nucleons and hyperons.

## ACKNOWLEDGEMENTS

I.L. is supported in part by the U.S. Department of Energy under grant DE-SC0023522. Work at Argonne is supported in part by the U.S. Department of Energy under contract DE-AC02-06CH11357. Discussions with Mikhail Bashkanov, Silas Beane, Takuya Nana-mura, Koji Miwa, Jen-Chieh Peng, Rik Yoshida and Nick Zachariou are gratefully acknowledged.

- 
- [1] V. G. J. Stoks, R. A. M. Klomp, M. C. M. Rentmeester, and J. J. de Swart, *Phys. Rev. C* **48**, 792 (1993).
  - [2] R. B. Wiringa, V. G. J. Stoks, and R. Schiavilla, *Phys. Rev. C* **51**, 38 (1995), arXiv:nucl-th/9408016.
  - [3] K. Miwa *et al.* (J-PARC E40), *Phys. Rev. C* **104**, 045204 (2021), arXiv:2104.13608 [nucl-ex].
  - [4] K. Miwa *et al.* (J-PARC E40), *Phys. Rev. Lett.* **128**, 072501 (2022), arXiv:2111.14277 [nucl-ex].
  - [5] T. Nanamura *et al.* (J-PARC E40), *PTEP* **2022**, 093D01 (2022), arXiv:2203.08393 [nucl-ex].
  - [6] J. Rowley *et al.* (CLAS), *Phys. Rev. Lett.* **127**, 272303 (2021), arXiv:2108.03134 [hep-ex].
  - [7] S. Acharya *et al.* (ALICE), *Phys. Lett. B* **805**, 135419 (2020), arXiv:1910.14407 [nucl-ex].
  - [8] S. Acharya *et al.* (ALICE), *Phys. Lett. B* **833**, 137272 (2022), arXiv:2104.04427 [nucl-ex].
  - [9] D. Chatterjee and I. Vidaña, *Eur. Phys. J. A* **52**, 29 (2016), arXiv:1510.06306 [nucl-th].
  - [10] L. Tolos and L. Fabbietti, *Prog. Part. Nucl. Phys.* **112**, 103770 (2020), arXiv:2002.09223 [nucl-ex].
  - [11] P. Demorest, T. Pennucci, S. Ransom, M. Roberts, and J. Hessels, *Nature* **467**, 1081 (2010), arXiv:1010.5788 [astro-ph.HE].
  - [12] J. Antoniadis *et al.*, *Science* **340**, 6131 (2013), arXiv:1304.6875 [astro-ph.HE].
  - [13] B. P. Abbott *et al.* (LIGO Scientific, Virgo), *Phys. Rev. X* **9**, 011001 (2019), arXiv:1805.11579 [gr-qc].
  - [14] B. P. Abbott *et al.* (LIGO Scientific, Virgo), *Phys. Rev. Lett.* **121**, 161101 (2018), arXiv:1805.11581 [gr-qc].
  - [15] T. A. Rijken, V. G. J. Stoks, and Y. Yamamoto, *Phys. Rev. C* **59**, 21 (1999), arXiv:nucl-th/9807082.
  - [16] V. G. J. Stoks and T. A. Rijken, *Phys. Rev. C* **59**, 3009 (1999), arXiv:nucl-th/9901028.
  - [17] T. A. Rijken, M. M. Nagels, and Y. Yamamoto, *Prog. Theor. Phys. Suppl.* **185**, 14 (2010).
  - [18] B. Holzenkamp, K. Holinde, and J. Speth, *Nucl. Phys. A* **500**, 485 (1989).
  - [19] J. Haidenbauer and U.-G. Meissner, *Phys. Rev. C* **72**, 044005 (2005), arXiv:nucl-th/0506019.
  - [20] H. Polinder, J. Haidenbauer, and U.-G. Meissner, *Nucl. Phys. A* **779**, 244 (2006), arXiv:nucl-th/0605050.
  - [21] J. Haidenbauer, S. Petschauer, N. Kaiser, U. G. Meissner, A. Nogga, and W. Weise, *Nucl. Phys. A* **915**, 24 (2013), arXiv:1304.5339 [nucl-th].
  - [22] J. Haidenbauer, U. G. Meißner, and A. Nogga, *Eur. Phys. J. A* **56**, 91 (2020), arXiv:1906.11681 [nucl-th].
  - [23] N. Ishii, S. Aoki, and T. Hatsuda, *Phys. Rev. Lett.* **99**, 022001 (2007), arXiv:nucl-th/0611096.
  - [24] H. Nemura *et al.*, *EPJ Web Conf.* **175**, 05030 (2018), arXiv:1711.07003 [hep-lat].
  - [25] S. R. Beane, P. F. Bedaque, T. C. Luu, K. Orginos, E. Pallante, A. Parreno, and M. J. Savage (NPLQCD), *Nucl. Phys. A* **794**, 62 (2007), arXiv:hep-lat/0612026.
  - [26] M. Illa *et al.* (NPLQCD), *Phys. Rev. D* **103**, 054508 (2021), arXiv:2009.12357 [hep-lat].
  - [27] J. Dai, H.-B. Li, H. Miao, and J.-Y. Zhang, (2022), arXiv:2209.12601 [hep-ex].
  - [28] S. R. Beane, D. B. Kaplan, N. Klco, and M. J. Savage, *Phys. Rev. Lett.* **122**, 102001 (2019), arXiv:1812.03138 [nucl-th].
  - [29] T. Mehen, I. W. Stewart, and M. B. Wise, *Phys. Rev. Lett.* **83**, 931 (1999), arXiv:hep-ph/9902370.
  - [30] T. Mehen, I. W. Stewart, and M. B. Wise, *Phys. Lett. B* **474**, 145 (2000), arXiv:hep-th/9910025.
  - [31] I. Low and T. Mehen, *Phys. Rev. D* **104**, 074014 (2021), arXiv:2104.10835 [hep-th].
  - [32] Q. Liu, I. Low, and T. Mehen, *Phys. Rev. C* **107**, 025204 (2023), arXiv:2210.12085 [quant-ph].
  - [33] M. Carena, I. Low, C. E. M. Wagner, and M.-L. Xiao, (2023), arXiv:2307.08112 [hep-ph].
  - [34] P. F. Bedaque and U. van Kolck, *Phys. Lett. B* **428**, 221 (1998), arXiv:nucl-th/9710073.
  - [35] D. B. Kaplan, M. J. Savage, and M. B. Wise, *Phys. Lett. B* **424**, 390 (1998), arXiv:nucl-th/9801034.

- [36] D. B. Kaplan, M. J. Savage, and M. B. Wise, Nucl. Phys. B **534**, 329 (1998), arXiv:nucl-th/9802075.
- [37] U. van Kolck, Nucl. Phys. A **645**, 273 (1999), arXiv:nucl-th/9808007.
- [38] A. D. Ballard and Y.-S. Wu, in *Cross disciplinary advances in quantum computing* (American Mathematical Society, Oxford, 2011) Chap. Cartan Decomposition and Entangling Power of Braiding Quantum Gates.
- [39] A. T. Rezakhani, Phys. Rev. A **70**, 052313 (2004).
- [40] D. W. L. Sprung, Phys. Rev. C **32**, 699 (1985).
- [41] <https://nn-online.org>, accessed: 2023-12-01.
- [42] M. M. Nagels, T. A. Rijken, and Y. Yamamoto, Phys. Rev. C **99**, 044002 (2019), arXiv:1408.4825 [nucl-th].
- [43] M. M. Nagels, T. A. Rijken, and Y. Yamamoto, Phys. Rev. C **99**, 044003 (2019), arXiv:1501.06636 [nucl-th].
- [44] O. Hashimoto and H. Tamura, Prog. Part. Nucl. Phys. **57**, 564 (2006).
- [45] Y. Yamamoto, T. Furumoto, N. Yasutake, and T. A. Rijken, Phys. Rev. C **90**, 045805 (2014), arXiv:1406.4332 [nucl-th].
- [46] S. Weinberg, Phys. Lett. B **251**, 288 (1990).
- [47] S. Weinberg, Nucl. Phys. B **363**, 3 (1991).
- [48] J. Haidenbauer, U.-G. Meißner, A. Nogga, and H. Le, Eur. Phys. J. A **59**, 63 (2023), arXiv:2301.00722 [nucl-th].
- [49] H. A. Bethe, Phys. Rev. **76**, 38 (1949).
- [50] S. R. Beane, E. Chang, S. D. Cohen, W. Detmold, H. W. Lin, T. C. Luu, K. Orginos, A. Parreno, M. J. Savage, and A. Walker-Loud, Phys. Rev. Lett. **109**, 172001 (2012), arXiv:1204.3606 [hep-lat].
- [51] Q. Liu and I. Low, to appear.
- [52] N. Hoshizaki, Prog. Theor. Phys. Suppl. **42**, 107 (1969).
- [53] Y. Afik and J. R. M. n. de Nova, Eur. Phys. J. Plus **136**, 907 (2021), arXiv:2003.02280 [quant-ph].
- [54] G. Aad *et al.* (ATLAS), (2023), arXiv:2311.07288 [hep-ex].
- [55] K. Miwa and T. Nanamura, private communications.